

Phase and Size Distribution of Polycyclic Aromatic Hydrocarbons in Diesel and Gasoline Vehicle Emissions

B. ZIELINSKA,^{*,†} J. SAGEBIEL,[†]
W. P. ARNOTT,[†] C. F. ROGERS,[†]
K. E. KELLY,[‡] D. A. WAGNER,[‡]
J. S. LIGHTY,[‡] A. F. SAROFIM,[‡] AND
G. PALMER[§]

*Division of Atmospheric Sciences, Desert Research Institute,
University and Community College System of Nevada,
2215 Raggio Parkway, Reno, Nevada 89512,
Department of Chemical and Fuels Engineering,
University of Utah, Kennecott Research Center, 100 S,
1495 E, Salt Lake City, Utah 84112, and
Hill Air Force Base, Ogden, Utah 84056*

Emission measurements were obtained for a variety of military vehicles at Hill Air Force Base (Ogden, UT) in November 2000 as part of a Strategic Environmental Research and Development Program. Aircraft ground support equipment vehicles using gasoline, diesel, and JP8 fuels were tested using chassis dynamometers under predetermined load. The exhaust from the tested vehicle was passed to a dilution tunnel where it was diluted 30–40 times and collected using Micro-Orifice Uniform Deposit Impactor (MOUDI) fitted with aluminum substrates, an XAD-coated annular denuder, and a filter followed by a solid adsorbent. All MOUDI substrates were analyzed for mass and for organic and elemental (EC) carbon by the thermal/optical reflectance method and for polycyclic aromatic hydrocarbons (PAHs) by GC/MS. Black carbon was measured with a photoacoustic instrument. The denuder and filter/solid adsorbent samples were analyzed for semivolatile PAH. Overall, there is more mass and higher EC contribution when the vehicle is run under higher load in comparison with the low load. However, older vehicles generally show more mass and EC emissions than newer vehicles, and there is a shift toward smaller particle sizes for the low load, which is most pronounced for newer vehicles. The particle-associated semivolatile PAHs and nonvolatile four-through six-ring PAHs are present predominantly on the submicron particles collected on MOUDI stages 0.1–0.18, 0.18–0.32, and 0.32–0.56 μm . For the low-load runs, the distribution of PAHs seems to be shifted toward smaller size particles. The gas-particle phase distribution of semivolatile PAHs depends also on the engine loading. For idle, not only are the more volatile two- and three-ring PAHs, from naphthalene to dimethylphenanthrenes, retained on the denuder portion, but also less volatile four-ring PAHs, such as fluoranthene and pyrene, are retained by the denuder at the 80–90% range, which implies that they are present

predominantly in the gas phase. In contrast, for engines under high loads, a much larger portion of three- and four-ring PAHs are partitioned to the particle phase.

Introduction

Polycyclic aromatic hydrocarbons (PAHs) constitute a broad family of compounds that are sometimes described as semivolatile organic compounds (SVOC). This term refers to the fact that PAHs are distributed between gas and particle phases. The factor of $\sim 10^7$ in the range of their vapor pressures is reflected in the fact that, at equilibrium at ambient temperature, two-ring naphthalene exists almost entirely in the gas phase, whereas five-ring PAHs and higher-ring PAHs are predominantly adsorbed on particles. The intermediate three- and four-ring PAHs are distributed between the two phases. However, the gaseous concentrations of these intermediate PAHs can be significantly reduced by their adsorption and absorption on various types of surfaces. Because of this phenomenon, the amount and type of particulate matter play an important role, together with temperature, in the vapor-particle partitioning of semivolatile organic compounds (1–4). Thus, the phase distribution of the PAH in the atmosphere is determined by the liquid phase (or subcooled liquid phase) vapor pressure of the individual species, by the amount and chemical nature of the particulate matter present (adsorption onto the aerosol surface and absorption into the aerosol organic matter), and by the temperature.

Diesel and gasoline-powered engines emit significant amounts of PAHs distributed between the gas and particle phases. However, the distribution of these PAHs in the diluted exhaust in relation to the engine work cycle (i.e., running under different loads or at idle) is not well-characterized. Since the amount and chemical nature of particulate matter (PM) produced by the given engine changes according to the work cycle, is the PAH phase and particle size distribution also cycle dependent? Are PAHs emitted by spark-ignition vehicles phase and particle size distributed at the same way as those emitted by diesel? This paper attempts to evaluate these questions.

Experimental Section

Sample Collection. The emission measurements were obtained for a variety of military vehicles at Hill Air Force Base (HAFB, Ogden, UT) in November 2000, as part of a Strategic Environmental Research and Development Program (SERDP) (5, 6). The selection of aircraft ground support equipment (AGE) vehicles is shown in Table 1 along with fuel type. More detailed description of the AGE vehicles, fuels, and run conditions could be found elsewhere (6).

Prior to vehicle testing, a dynamic blank was run on the system using the same dilution tunnel, clean air, and sampling equipment as for the actual experiments. AGE vehicles, with the exception of the Jammer were tested using chassis dynamometers under predetermined load. It was not possible to operate the Jammer on the dynamometer; therefore, it was only tested under idle conditions. The experimental conditions are presented in Table 2. In Table 2, a single entry under engine load (such as 53%/72 kW) indicates that the engine load remained constant throughout the run. Multiple entries (such as 23, 9%/24, 9 kW) indicate that the engine load was set at 23% for half of the run and 9% for the other half of the run (runs were always divided equally between all dyno settings). The exhaust from the tested vehicle was

* Corresponding author phone: (775)674-7066; fax: &(775)674-7060; e-mail: barbz@dri.edu.

[†] Desert Research Institute.

[‡] University of Utah.

[§] Hill Air Force Base.

TABLE 1. Aircraft Ground Support Equipment Tested in the HAFB Experiment

vehicle type ^a	fuel type	engine manufacturer	engine displacement	exhaust treatment
1993 Ford F-350	gasoline	Ford	5.8 L	catalytic converter
1996 Dodge Bobtail	diesel	Cummins	5.9 L	none
1986 Jeep Bobtail	diesel	Nissan	4.4 L	none
1992 Jammer	JP-8 aviation fuel	HATZ	1.27 L	none

^a Bobtail vehicles tow aircraft, and Jammers lift munitions into aircraft.

TABLE 2. Vehicle and Dilution Conditions for HAFB Tests^a

run (min)	AGE	engine speed (rpm)	engine load (%/kW)	torque (N m)	dilution ratio	RH (%)	temp (°C)
60	Ford F350	2450	53/72	224	1:34.2	2–31	22–24
60	Ford F350	2450	53, 43, 32, 21, 11/72, 58, 43, 28, 14	224, 179, 134, 90, 45	1:37.6	13–32	20–26
60	Dodge Bobtail	700	idle	idle	1:33.5	11–13	27–28
60	Dodge Bobtail	1500	95, 81, 54, 27/96, 72, 48, 24	759, 616, 411, 206	1:31.7	15–21	24–26
60	Dodge Bobtail	1500	27/24	206	1:30.3	18–22	22–24
60	Dodge Bobtail	1500	27/24	206	1:30.4	23–29	18–22
45	Jeep Bobtail	1700	23/24	411	1:31.8	23–31	19–24
20	Jeep Bobtail	1700	23/24	411	1:31.8	10–22	24–26
20	Jeep Bobtail	1700	23, 9/24, 9	411, 164	1:31.1	9–16	26–28
20	Jeep Bobtail	1700*	93, *, 23/87, *, 48	1640, *, 822	1:42.0	8–20	24–27
30	Jammer	2500	idle	idle	1:32.1	14–29	16–26
30	Jammer	2500	idle	idle	1:31.3	2–14	27–33

^a Key: *, acceleration during the middle of the test; RH, relative humidity.

passed to the DRI dilution tunnel, which is based on the design of Hildemann et al. (7). The inlet to the dilution sampler was a 3.2m long line heated to 150 °C. This sample stream was diluted by air that had passed through a HEPA filter, desiccant, and activated carbon beds. The dilution ratios for each run are shown in the third to last column of Table 2. The diluted sample was allowed to equilibrate in the residence chamber for approximately 80 s before being passed to the aerosol characterization instruments. The temperature and the relative humidity in the dilution sampler ranged from 18 to 33 °C and from approximately 5% to 31%, respectively, depending on engine and ambient conditions. The dilution sampler flow supplied four sampling trains, two of which (nos. 1 and 2) were fitted with Bendix-Unico 240 cyclones (8), which provide a 50% cut-point of 2.5 μm aerodynamic diameter at a volumetric flow rate of 113 L/min. The remaining two sampling trains (nos. 3 and 4) did not contain size-classifying devices. Sampling trains 1 and 2 supplied the DRI fine particulate/semivolatile organic compound sampler (FP/SVOC) and an annular denuder (both described below), respectively. A Micro-Orifice Uniform Deposit Impactor (MOUDI) and a photoacoustic instrument for black carbon particulate measurement were connected to sampling train 4.

Sampling Methods. The gas-phase components of the semivolatile PAHs were collected using a sorbent-coated annular denuder (9). The denuder sampler, purchased from the University Research Glassware Corporation (URG, Chapel Hill, NC), consisted of three stages; the first stage was an 8-channel denuder section (52 mm o.d., 600 mm length) coated with polystyrene-divinylbenzene resin XAD-4, which strips the gas-phase species from the airstream before collection of the particles on a second stage, consisting of a 47-mm Teflon-impregnated glass fiber (TIGF, T60X20) filter. The third stage consisted of polyurethane foam plugs (1 in. diameter) in combination with the 5 g of adsorbent resin XAD-4 (PUF/XAD/PUF “sandwich” cartridge) that was placed downstream of the filter to assess “blow off” or volatilization loss of semivolatile PAHs from the particles. The denuder XAD coating was performed by Dr. Lara Gundel of the University of California, Berkeley. In parallel, a medium-volume DRI fine particulate/semivolatile organic compound

(FP/SVOC) sampler, using 90 mm TIGF (T60X40) filters backed by the PUF/XAD/PUF “sandwich” cartridge (10 g of XAD-4 resin between two 2-in. PUF plugs) was employed. The flow was set at approximately 90 L/min for the denuder and at 100 L/min for the FP/SVOC sampler.

Prior to sampling, the XAD-4 resin was cleaned by Soxhlet extraction with methanol followed by dichloromethane (CH₂-Cl₂), each for 48 h. The cleaned resin was then dried in a vacuum oven heated at 40 °C and stored in sealed glass containers in a clean freezer. The PUF plugs were cleaned by Soxhlet extraction with acetone followed by extraction with 10% diethyl ether in hexane, as described in U.S. EPA Method TO-13. Prior to sampling, XAD-4 resin and PUF plugs were loaded into the glass sampling cartridges. The TIGF filters were cleaned by sonication in methanol for 10 min (twice), followed by two more 10-min sonications in CH₂Cl₂. The filters are then dried, placed in clean aluminum foil, and labeled. Each batch of precleaned XAD-4 resin and ~10% of precleaned PUF plugs and TIGF filters were checked for purity by solvent extraction and GC/MS analysis of the extracts. The sampling flow rates were checked before and after sampling. After sampling, the filters were placed in clean aluminum foil, and the PUF/XAD/PUF sandwich cartridges were also wrapped in aluminum foil and stored at ice temperature until transported to a laboratory freezer.

Micro-Orifice Uniform Deposit Impactor (MOUDI). A MOUDI sampler was used in this sampling campaign; it was fitted with aluminum media for thermal/optical reflectance (TOR) carbon analyses. In the configuration we used, the top stage (which would nominally be 5.6 μm) was greased with high vacuum grease to remove any larger particles and prevent particle bouncing. The stages at 3.2, 1.8, 1.00, 0.53, 0.32, 0.18, 0.096, and 0.049 μm were used in the normal manner, with the after-filter collecting particles smaller than 0.049 μm. The MOUDI operated at a flow rate of 30 L/min.

Photoacoustic Black Carbon Measurements. Black carbon was measured continuously during all dyno runs with the photoacoustic instrument developed by Arnott and coworkers (10, 11). Sample air is pulled continuously through an acoustical resonator and is illuminated by laser light that is periodically modulated at the acoustical resonance frequency. Light absorption is manifested in particle heating,

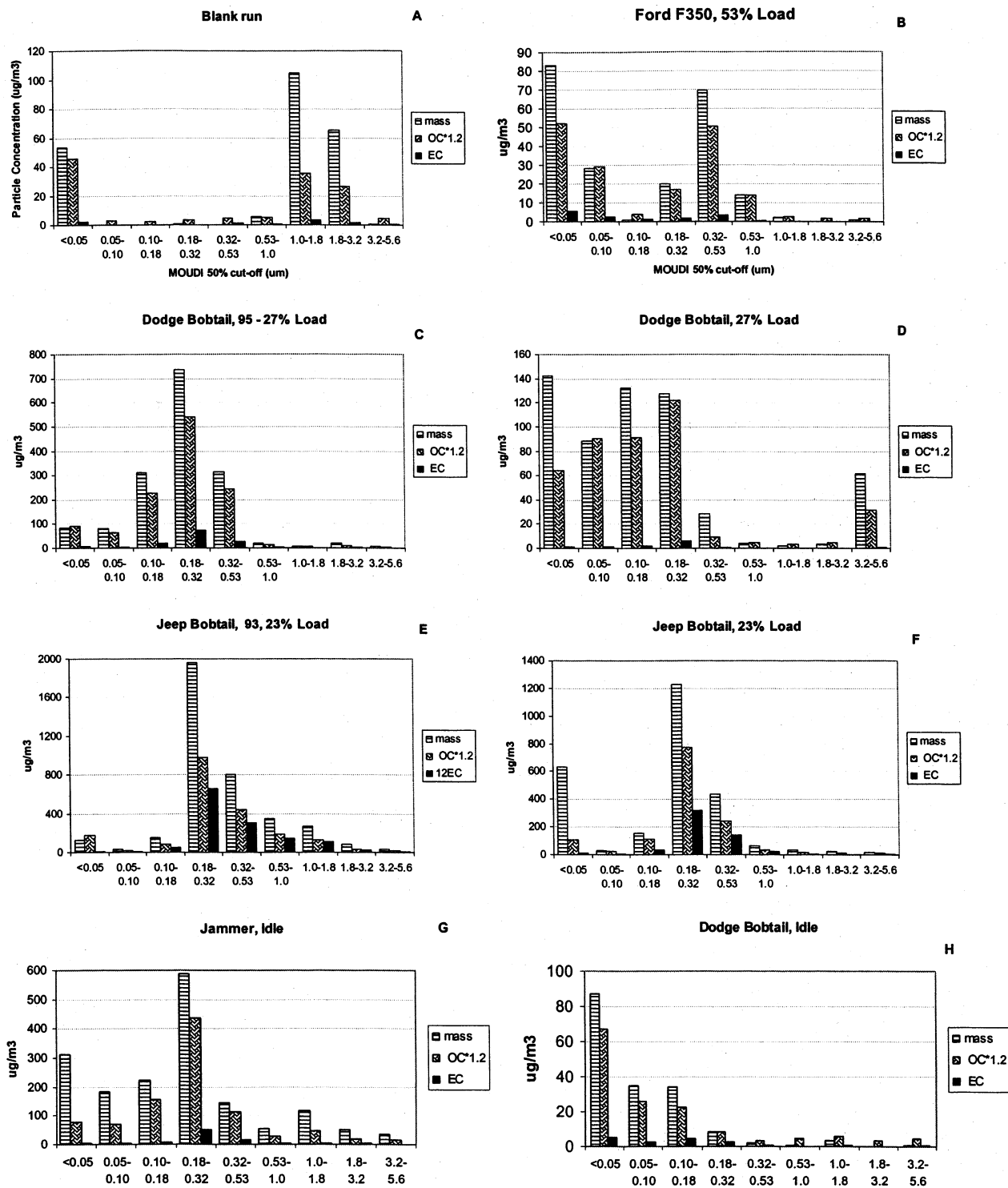


FIGURE 1. Distribution of mass, OC, and EC over MOUDI stages for selected runs. (A) system blank; (B) Ford F350, high (53%) load; (C) 1996 Dodge Bobtail, variable (95, 81, 54, and 27%) load; (D) 1996 Dodge Bobtail, low (27%) load; (E) 1986 Jeep Bobtail, variable (93, 23%) load; (F) 1986 Jeep Bobtail, low (23%) load; (G) 1992 Jammer, idle; (H) 1996 Dodge Bobtail, idle.

and this heat transfers rapidly to the surrounding air, inducing pressure fluctuations that are picked up with a microphone on the resonator. Microphones have a very large dynamic range (at least 6 orders of magnitude), so black carbon measurements can be made over a large dynamic range with these instruments. Aerosol light absorption occurs throughout the entire particle volume for combustion particles, so black carbon aerosol mass concentration is found to vary in direct proportion with light absorption. The photoacoustic instrument modified for this work (12) operates at a

convenient wavelength of 1047 nm where gaseous interference is not a problem and where a laser source is available that allows for direct electronic modulation of the power at the resonator frequency.

Black carbon measurements of vehicle emissions were accomplished with the photoacoustic instrument sampling from the DRI dilution system. Sample air was continuously pulled through the instrument at a rate of 1 L/min. The sample change time for the instrument was approximately 1 s, although data were gathered at an electronic sampling rate

TABLE 3. MOUDI Mass, Organic Mass (OC*1.2), and EC Data ($\mu\text{g}/\text{m}^3$)

stage no.	cutoff (μm)	blank			Dodge Bobtail, high			Dodge Bobtail, low			Dodge Bobtail, low ^a			Jeep Bobtail, low			Jeep Bobtail, high		
		mass	OC	EC	mass	OC	EC	mass	OC	EC	mass	OC	EC	mass	OC	EC	mass	OC	EC
1	3.2	0.7	4.6	0.4	6.7	3.5	1.2	61.4	31.8	0.5	7.0	4.7	0.2	21.0	11.2	3.4	32.8	21.3	8.1
2	1.8	65.4	26.6	1.9	21.8	8.8	2.4	3.5	4.5	0.2	3.5	3.4	0.1	738.4	274.8	12.0	84.9	44.0	27.2
3	1	104.7	35.3	3.4	7.3	5.6	1.5	1.8	3.3	0.1	3.5	3.9	0.2	36.3	25.6	11.1	271.9	154.8	109.9
4	0.56	5.8	5.2	0.5	20.1	14.1	3.1	4.1	4.6	0.2	4.1	3.6	0.2	291.9	149.1	45.4	345.2	225.6	141.9
5	0.32	0.0	4.7	1.0	315.3	241.5	25.9	28.7	9.5	0.4	5.8	6.3	0.4	469.4	313.7	144.4	798.4	523.0	303.8
6	0.18	0.7	3.2	0.1	736.1	541.5	75.3	127.5	122.1	6.1	158.4	151.3	6.4	1194.5	911.5	278.6	1955.6	1177.7	655.3
7	0.1	0.0	2.4	0.0	309.2	227.0	21.9	132.2	91.5	1.9	142.0	156.3	2.9	173.6	155.0	33.4	152.4	100.7	47.4
8	0.056	0.0	2.6	0.0	82.0	64.8	3.6	88.3	90.3	1.1	101.7	82.7	1.6	47.7	44.4	3.6	30.9	25.0	4.8
AF		53.8	45.9	2.4	83.2	91.8	7.1	142.1	63.9	1.5	47.9	84.2	2.2	158.4	123.0	7.3	129.2	217.3	11.0

^a Duplicate run.

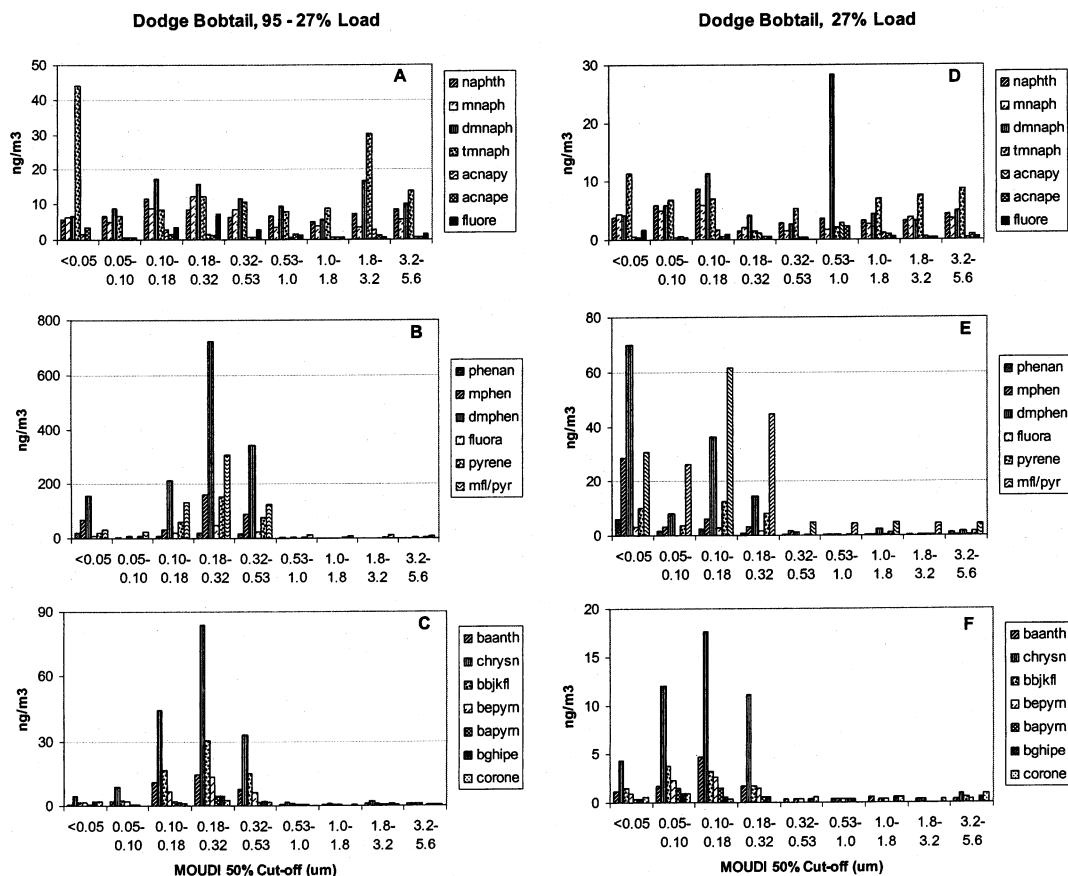


FIGURE 2. Distribution of PAH over MOUDI stages for 1996 Dodge Bobtail runs. (A–C) variable (95, 81, 54, and 27%) load; (D–F) low (27%) load.

of between 3 and 30 s. The DRI dilution system introduces a time constant of around 80 s.

Analysis Methods. The SVOCs collected on each denuder-filter-PUF/XAD/PUF sampling train were extracted separately with high-purity, HPLC grade solvents. The denuder portion was extracted with cyclohexane immediately following the sample collection. Approximately 200 mL of cyclohexane was poured into the denuder section, which had been capped at one end. The other end was capped, and the denuder was manually inverted about 10 times. The solvent was drained and the procedure repeated two more times, using *n*-hexane for the last extraction. The PUF/XAD plugs were microwave-extracted with 10% diethyl ether in hexane (13), and the filters were microwave-extracted with dichloromethane. Prior to extraction, the following deuterated internal standards were added to each PUF, filter, and XAD sorbent: naphthalene-*d*₈, acenaphthylene-*d*₈, phenanthrene-*d*₁₀, anthracene-*d*₁₀, chrysene-*d*₁₂, fluoranthene-*d*₁₀, pyrene-*d*₁₀, benz[*a*]anthracene-

*d*₁₂, benzo[*e*]pyrene-*d*₁₂, benzo[*a*]pyrene-*d*₁₂, benzo[*k*]fluoranthene-*d*₁₂, and benzo[*ghi*]perylene-*d*₁₂. The extracts were concentrated by rotary evaporation at 20 °C under gentle vacuum to ~1 mL and filtered through 0.20 μm of Anotop (Whatman International, Ltd.), rinsing the sample flask twice with 1 mL of CH_2Cl_2 each time. Approximately 50 μL of acetonitrile was added to the sample, and CH_2Cl_2 was evaporated under a gentle stream of nitrogen. The final volume was adjusted to 1 mL with acetonitrile. The sample was then analyzed by electron impact (EI) GC/MS technique, using an Ion Trap Varian Saturn 2000, operating in the selected ion storage (SIS) mode. Injections (1 μL) were made in the splitless mode onto a 30 m \times 0.25 mm i.d. CPSil 8 fused-silica capillary column (Varian, Inc.). Identification and quantification of the SVOC was made by SIS, monitoring the molecular ion of each SVOC and deuterated SVOC. Calibration curves for the GC/MS/SIS quantification were made for the molecular ion peaks of the SVOC using the corresponding

TABLE 4. PAHs and Their Mnemonics

Mnemonic	PAH
naphth	naphthalene
mnaph	methylnaphthalenes (2 isomers)
biphen	biphenyl
dmenaph	dimethylnaphthalene (6 isomers)
mebiph	methylbiphenyls (3 isomers)
tmenaph	trimethylnaphthalenes (12 isomers)
acnapy	acenaphthylene
acnape	acenaphthene
fluore	fluorene
phenan	phenanthrene
meflu	methylfluorenes (3 isomers)
xanone	xanthone
acquone	acenaphthenequinone
mephen	methylphenanthrene (5 isomers)
anrquone	anthraquinone
dmephen	dimethylphenanthrene (7 isomers)
antra	anthracene
fluora	fluoranthene
pyrene	pyrene
bntiop	benzonaphthothiophene
mefl/py	methyl pyrene/methyl fluoranthene (6 isomers)
bzcphen	benzo[c]phenanthrene
baanth	benzo[a]anthracene
chrysn	chrysene/triphenylene
bzantone	benzanthrone
baa7_12	benzo[a]anthracene-7,12-dione
chry56m	5+6-methylchrysene
bbjkfl	benzo[b+j+k]fluoranthene
bepyrn	benzo[e]pyrene
peryle	perylene
bapyrn	benzo[a]pyrene
incdpy	indeno[1,2,3-cd]pyrene
bghepe	benzo[ghi]perylene
dbanth	dibenz[ah+ac]anthracene
corone	coronene

deuterated species (or the deuterated species most closely matched in volatility and retention characteristics) as internal standards. NIST SRM 1647d (certified PAH), with the addition of deuterated internal standards and authentic standards of compounds not present in the SRM, were used to make calibration solutions.

All aluminum MOUDI substrates were analyzed for mass and for organic (OC) and elemental (EC) carbon by thermal/optical reflectance (TOR) method as described previously (14). The TOR analysis used one-fourth of an aluminum substrate, and no correction for pyrolysis was applied to these samples. The remaining three-fourths of selected MOUDI samples was spiked with deuterated PAH standards, extracted by sonication with dichloromethane (repeated 3 times), concentrated to 25 μ L, and analyzed for PAH, as described above.

All data discussed below are not corrected for dilution. The phase and size distribution of PAHs discussed in this paper relates to the diluted exhaust and may not be valid for tailpipe conditions. Therefore, the correction for dilution might be potentially misleading.

Results

MOUDI Mass and Carbon Data. With the exception of the quartz after-filter, all OC/EC data were obtained from aluminum foil by the TOR method (14). However, due to the reflective nature of aluminum foil, it was not possible to apply the pyrolysis correction for these samples. Thus, the concentrations of EC might be slightly overestimated. Although MOUDI EC data correlate very well with BC data obtained by the continuous photoacoustic method (W. Arnott, unpublished results) for the same runs (slope = 0.99 and $r^2 = 0.97$), there is a significant difference between BC

and EC concentrations for the runs with low mass emissions, as shown later.

Figure 1 shows the distribution of mass, organic carbon $\times 1.2$ (to account for hydrogen mass), and elemental carbon between individual MOUDI stages for the dynamic system blank and for the diluted exhaust from the AGS vehicles, run under different conditions (see Table 2 for the run description). Although the dynamic system blank sample (Figure 1A) obtained prior to all vehicle runs shows some mass, the distribution of mass between different MOUDI stages is different than for the exhaust samples. For the system blank the majority of mass is found on the 1.0–1.8 and 1.8–3.2 μ m stages, indicating that some accumulation mode particles are being reentrained from the dilution tunnel walls and/or sampling lines when clean air is run through the system. The gasoline vehicle diluted exhaust from a run under high (53%) load (Figure 1B) shows very different mass distribution, with the majority of mass collected on 0.32–0.53, 0.18–0.32, 0.05–0.1, and <0.05 μ m stages. The mass is composed mostly of OC, with very little EC present.

For the two diesel vehicles tested on the dynamometer, 1996 Dodge Bobtail and 1986 Jeep Bobtail, there is overall more mass and higher EC contribution when the vehicle engine is run under higher and variable load (Figure 1C,E) in comparison with the low load (Figure 1D,F). However, the older vehicle shows in general more mass and EC emissions than the newer vehicle (EC constitutes 35% and 26% of TC for the Jeep tested under high, variable, and low load, respectively, as compared with 11% and 3% for Dodge). Also, there is a shift toward smaller particle sizes for the low load, which is the most pronounced for the newer vehicle, the 1996 Dodge Bobtail. Figure 1, panels G and H, shows the distribution of mass and OC/EC for the two vehicles running under idle conditions, a 1992 Jammer and 1996 Dodge Bobtail, respectively. The Jammer exhaust contains more mass than the Dodge Bobtail, but the emissions from both vehicles is mostly OC.

The quartz after-filters (<0.056 μ m) contain significant amount of mass for all runs. However, since the mass was obtained from the gravimetric analysis of quartz filters, there are two factors that can make these measurements inaccurate: (i) the quartz filter is prone to a positive sampling artifact (i.e., adsorption of gaseous organic compounds on the filter during sampling); (ii) some particle bouncing could have occurred during sampling. Since the main constituent of the after filter mass is OC, with very little of EC, this supports the first assumption.

The correlation of particle mass with the sum of EC + OC $\times 1.2$ for all individual stages (excluding quartz after filters) and all vehicle runs (excluding blank run) show an excellent relationship; the slope of the trend line is equal to 0.96 and $r^2 = 0.99$. Thus, the particulate matter emitted by vehicles tested during this experiment consists mostly of carbonaceous species, with small amount of sulfates and trace elements (6).

Table 3 shows the distribution of the particle mass and OC/EC between individual MOUDI stages for runs selected for PAH analysis in the diluted vehicle exhaust. Since two Dodge Bobtail runs under 27% load were replicates, they were combined in order to obtain sufficient mass for these analyses.

MOUDI PAH Data. Figure 2A–C shows the distribution of PAH between the MOUDI stages collected from the diluted Dodge Bobtail exhaust for a complete run that included four engine settings (95, 81, 54, 27%) and Figure 2D–F has one engine setting (low load 27%). Although it is generally assumed (15) that the aluminum foil has very low affinity for gaseous organic compounds and thus is not prone to positive sampling artifacts, it is clear from this figure that the gas-phase PAHs (Figure 2A,D) are present in measurable amounts

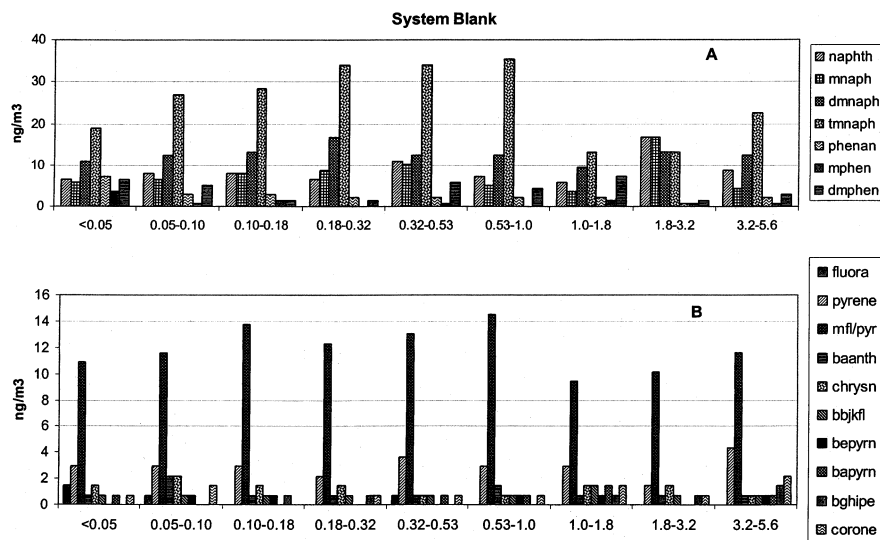


FIGURE 3. Distribution of PAH over MOUDI stages for system blank. (A) gas-phase PAH; (B) semivolatile and particle phase PAH.

in all stages. Naphthalene, methylnaphthalenes, and dimethylnaphthalenes are present in very high concentrations in spark-ignition and diesel vehicle exhaust and are even few orders of magnitude higher than particle-associated four- and five-ring PAH. These gas-phase PAHs are distributed randomly between all stages, which indicates their nonspecific adsorption, most likely on the particles collected on the various MOUDI stages (i.e., positive sampling artifact). The particle-associated semivolatile PAHs (Figure 2B,E) and nonvolatile four- through six-ring PAHs (Figure 2C,F) are present predominantly on the submicron particles collected on MOUDI stages 0.18–0.32, 0.32–0.56, and 0.1–0.18 μm (see Table 4 for the explanation of mnemonics). For the low-load runs (27%), the distribution of PAH seems to be shifted toward smaller size particles, which is consistent with mass and OC distribution. In addition, the concentrations of PAH are much lower in low-load runs.

A comparison of the diesel samples in Figure 2 with the dynamic system blank in Figure 3 showed that the blank run exhibits much lower PAH concentrations distributed randomly between all stages. Since the dynamic system blank was run prior to all vehicle runs, using the same dilution tunnel, dilution air, and sampling equipment, it is possible that some very small amount of particles and semivolatile material remaining from previous experiments (despite the throughout system cleaning) was released from the walls of the dilution tunnel and/or sampling lines. Although most of the mass for blank run is contained on the larger particles (see Figure 1A), PAHs are distributed randomly between all particle sizes.

Denuder PAH Data. Figure 4 shows the percentage of PAH present on the denuder portion (coated with XAD resin) of the annual denuder for 1996 Dodge Bobtail run under idle (Figure 4A), low load (27%, Figure 4B), and variable (95, 81, 54, and 27%) load (Figure 4C) conditions in relation to total PAH present on denuder + filter + PUF/XAD/PUF cartridge. The PAH are shown according to their elution order from a nonpolar capillary column (CPSil 8, 5% phenylmethylsilicone), which separates PAH according to their volatility. The most volatile and most abundant PAH (naphthalene and methylnaphthalenes) shows significant break through the denuder (approximately 20% and 10%, respectively), as Figure 4 shows. The flow rate through our denuder was calculated based on Possanzini model (16) to be optimal for phenanthrene (99.5% efficiency) at 92 L/min. Thus, PAHs more volatile than phenanthrene might pass through the denuder with this flow rate. However, the lower flow rate could have

resulted in a particle loss to the denuder walls and evaporative losses of more volatile PAHs from particles. The diffusional losses depend on the particle residence time and are important for smaller particles ($d_p < 0.01 \mu\text{m}$). As it can be seen from Figure 2C,F, the higher molecular weight (mw) PAHs (from BaA to coronene) are present in significant amounts on small particles (0.05–0.1 μm MOUDI cutoff stage), especially for a low load run (27%). Consequently, some diffusional particle losses might have occurred for low load or idle runs and, as it can be seen in Figure 4, the gas-phase concentrations of some higher mw PAH, such as BeP or benzo[ghi]perylene are higher than expected.

Evaporative losses are important for higher volatility compounds that can evaporate from particles during their residence time in the denuder, as surrounding gases are removed and the equilibrium is disturbed (17). Thus, the transit time through the sorbent-coated section should be short enough to limit evaporation of semivolatile PAHs from particles (≤ 0.3 s recommended). For 92 L/min flow rate and 5.2 cm \times 60 cm 8-channel denuder used in this work, the transit time was approximately 0.3 s.

It can be seen from Figure 4 that the gas-particle distribution for these diesel runs depends on the engine loading. For idle (Figure 4A), the more volatile two- and three-ring PAHs, from dimethylnaphthalenes to dimethylphenanthrenes, are retained entirely on the denuder portion, and the less volatile four-ring PAHs, such as fluoranthene and pyrene, are retained by the denuder at the 80–90% range. These results imply that these PAHs are present predominantly in the gas phase. In contrast, for engines under high, variable load (Figure 4C) a much larger portion of three- and four-ring PAHs is partitioned to the particle phase. The low-load results (27%, Figure 4B) are clearly situated between these two extremes. The nonvolatile five-ring PAHs, such as benzo[b+j+k]fluoranthene, BaP, BeP, or benzo[ghi]perylene are present predominantly on the filter for all runs.

The partitioning of SVOC, such as PAHs, between the gas- and particle-bound phases has been parametrized by the partition coefficient, K_p ($\text{m}^3 \mu\text{g}^{-1}$) according to the following relationship (2, 5, 18):

$$K_p = [C_p/TSP]/C_g$$

where TSP is the concentration of total suspended particulate matter ($\mu\text{g m}^{-3}$), and C_p and C_g are the measured particle- and gas-phase concentrations of the analyte of interest, respectively. The mechanism of gas/particle (G/P) partition-

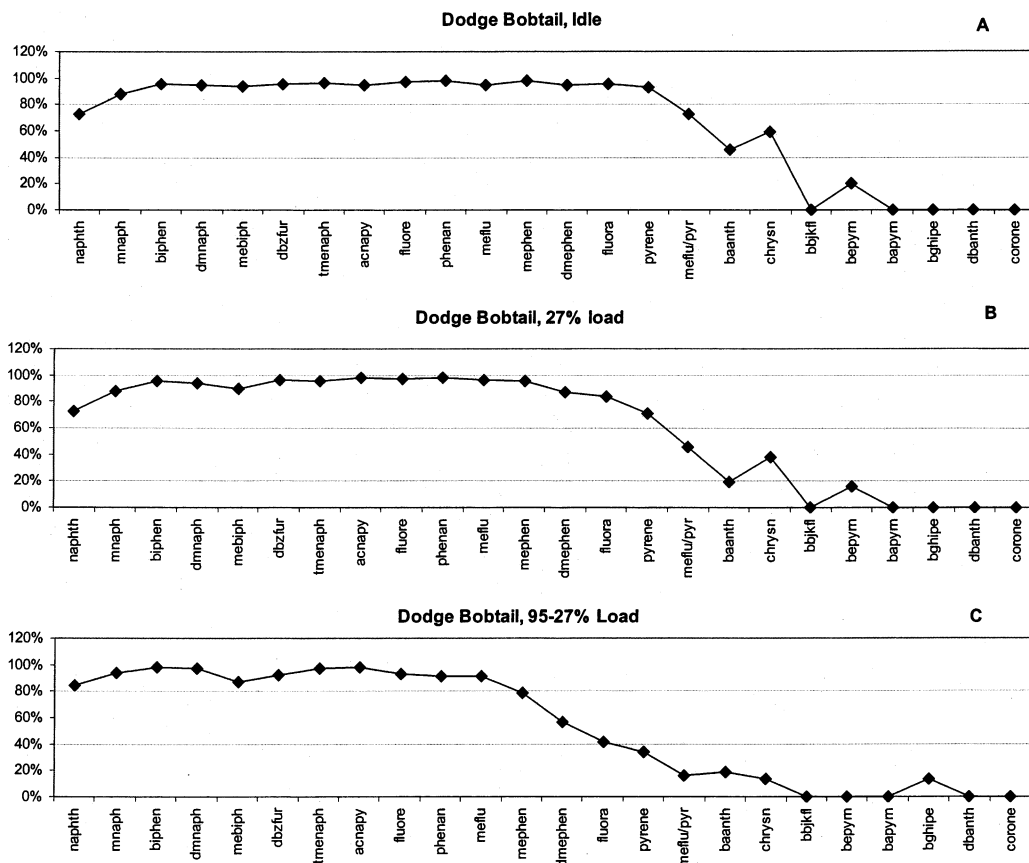


FIGURE 4. Percentage of PAH present on the XAD-covered denuder stage for 1996 Dodge Bobtail runs. (A) idle; (B) low load (27%); (C) variable (95, 81, 54, and 27%) load.

TABLE 5. Mass, EC, BC, $OC \times 1.2$, and C_p/C_g Data for Fluoranthene and Pyrene

vehicle	load (%)	mass ($\mu\text{g}/\text{m}^3$)	EC ($\mu\text{g}/\text{m}^3$)	BC ($\mu\text{g}/\text{m}^3$)	$OC \times 1.2$ ($\mu\text{g}/\text{m}^3$)	$OC \times 1.2/BC$	C_p/C_g , fluoranthene	C_p/C_g , pyrene	total particle concn (cm^{-3}) ^b	surface area ($\mu\text{m}^2 \text{cm}^{-3}$)
Ford F-350	53	218.4	15.7	2.5	69.8	27.9	0.27	0.59	2.15E+05	918.02
Ford F-350	53, 43, 32, 21, 11	40.2	3.5	0.25	54.7	219.0	0.02	0.08		
Dodge Bobtail	idle	168.3	16.5	8.5	144.8	17.0	0.05	0.07	9.42E+05	4146.0
Dodge Bobtail	95, 81, 54, 27	1581.6	142.0	79.88	1198.6	15.0	1.43	1.95	1.68E+06	38643.45
Dodge Bobtail	27	589.6	12.0	21.67	421.5	19.4	0.19	0.41	1.49E+06	10861.15
Dodge Bobtail	27	474.0	14.3	18.39	496.3	27.0	0.24	0.53	1.62E+06	13209.21
Jeep Bobtail	23	1686.9	519.8	464.06	1027.0	2.2	0.31	0.39	7.16E+05	24308.11
Jeep Bobtail	23	2622.1	553.5	609.21	1604.7	2.6	0.38	0.59	9.08E+05	37012.27
Jeep Bobtail	23,9	3131.2	539.2	525.59	2008.3	3.8	0.38	0.47	1.13E+06	34740.43
Jeep Bobtail	93,23	3801.2	1309.5	na	2489.5	1.9 ^a	0.57	1.37		
Jammer	idle	881.7	199.5	169.19	633.6	3.7	0.13	0.18	8.87E+05	23005.34
Jammer	idle	1702.4	96.7	151.79	1154.9	7.6	0.11	0.16	7.97E+05	17557.77
Jammer	idle	na ^c	na	50.24	na	na	0.08	0.09		

^a EC was used for obtaining this ratio. ^b Obtained from ref 6, without correction for dilution. For Dodge Bobtail run under variable (95, 81, 54, and 27%) load, the arithmetic mean of total particle concentration measured during each load setting is presented. ^c na, not available.

ing includes adsorption onto the aerosol surface and absorption into the aerosol organic matter layer (2, 3, 19, 20). Although the relative importance of these two mechanisms remain unclear, several investigators have suggested that G/P partitioning is primarily absorptive in nature and can be described by the gas-liquid interaction processes under many conditions (2, 3, 21-23). However, it has been recently argued that adsorption onto aerosol soot carbon dominates G/P partitioning of PAH and that absorption may account for less than 10% of total PAH in the particulate phase (24). Since our dynamometer measurements include several vehicles and test cycles that produced different amount of soot and organic carbon fractions, it was interesting to compare the G/P partitioning of PAH for these runs.

Table 5 lists $OC \times 1.2$, EC, and black carbon (BC, obtained by the photoacoustic method) concentrations in the diluted exhaust of all vehicle's runs listed in Table 2. Also, the ratio of particle to gas phase concentrations (C_p/C_g) for fluoranthene and pyrene are listed. C_g values are obtained from the XAD-coated denuder section, whereas C_p represents the sum of filter and PUF/XAD/PUF concentrations. As mentioned before, EC and BC are highly correlated for these runs. However, since no correction for pyrolysis was applied to the TOR method (due to the reflective nature of aluminum foil), the EC values might be slightly overestimated, especially for the runs with low EC content and high OC content. Thus, the BC values reflect probably more correctly the emissions soot content than EC values. The $OC \times 1.2/BC$ ratio is also

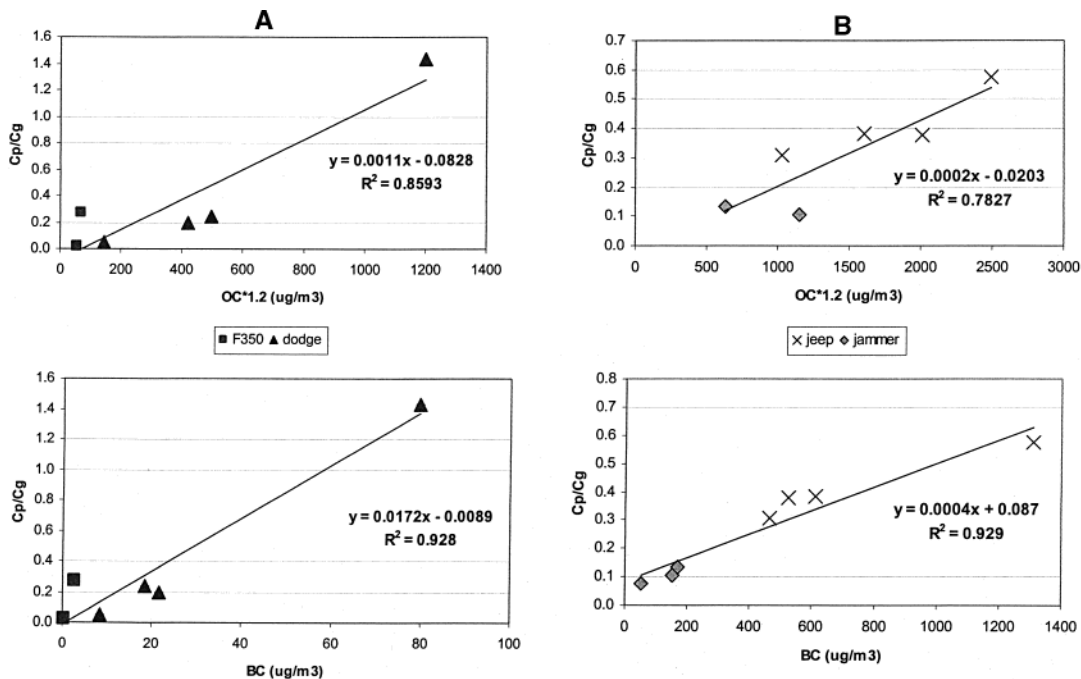


FIGURE 5. Relations between fluoranthene C_p/C_g , BC, and $OC \times 1.2$ for Ford 350 and Dodge Bobtail (A) and for Jeep Bobtail and Jammer (B).

listed in Table 5. Since BC was not available for the Jeep Bobtail run under 93% and 23% load, EC was used for deriving this ratio. As it could be seen from Table 5, for high EC content, both BC and EC values are very similar.

As Table 5 shows, all runs could be divided into two groups based on the $OC \times 1.2/BC$ ratio. The first group is characterized by a high $OC \times 1.2/BC$ ratio (from 15 to 219) and consists of relatively “clean” newer vehicles (gasoline 1993 Ford F350 and diesel 1996 Dodge Bobtail). The second group with a low $OC \times 1.2/BC$ ratio (from 2 to 7.6) consists of more “dirty” older vehicles (i.e., 1986 Jeep Bobtail and 1992 Jammer). For fluoranthene, both groups show good correlations of C_p/C_g with BC and $OC \times 1.2$, as shown in Figure 5A,B for the first and second group, respectively (pyrene shows similar correlations). These correlations seem to suggest that particle-bound PAH is related more strongly with BC than OC.

The highest C_p/C_g ratio for both fluoranthene and pyrene (1.4 and 1.9, respectively) corresponds to the 1996 Dodge Bobtail, run under four engine loads (Table 5 and Figure 5). Kelly et al. (6) measured the particle size distribution and particle counts by scanning mobility particle sizer (SMPS) during most of the same runs; the particle number concentrations are shown in the second to last column of Table 5. The results of these measurements for diesel Dodge Bobtail, run under variable load conditions (95, 81, 54, and 27%) clearly shows the increase in particle number concentrations and the shift to larger particle diameter (CMD, count median diameter) with the increasing vehicle load. Figure 6A shows the correlation of C_p/C_g with total particle concentrations for fluoranthene (pyrene looks similar). Although some correlation could be seen from this graph, it is obvious that the C_p/C_g ratio is not entirely driven by the integrated particle number concentrations. Assuming the spherical particle shape, we calculated the particle surface area, shown in Table 5, based on the SMPS measurements. The correlations between C_p/C_g and these surface areas is shown in the Figure 6B. This graph shows that the surface area was not able to collapse the data to a single linear relationship, and we again obtained two families of curves.

The data presented in Table 5 and Figures 5 and 6 do not allow us to determine if adsorptive or absorptive mechanisms

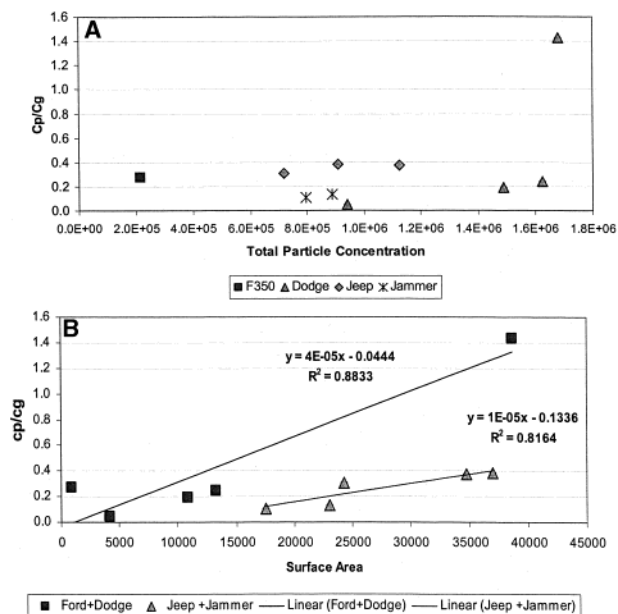


FIGURE 6. Relations between C_p/C_g and total particle number concentration (A) and particle surface area (B) for fluoranthene.

dominate the gas-particle partitioning of PAH, although they do suggest a stronger connection of BC with particle-bound PAH than with OC.

The exhaust from all vehicles tested on the dynamometer was diluted 30–40 times and allowed to equilibrate for approximately 80 s prior to collection (see Table 2). Since it has been shown (25) that under warm conditions (as used in this study, see Table 2) the equilibrium between gas- and particle-phase PAHs is reached very quickly, on the order of several seconds, we assume that all measurements presented here were made under equilibrium conditions. However, these are the conclusions of direct source sampling with diluted, scrubbed air. Further dilution and transformations may occur in the atmosphere to adjust this picture of the gas- and particle-phase distribution.

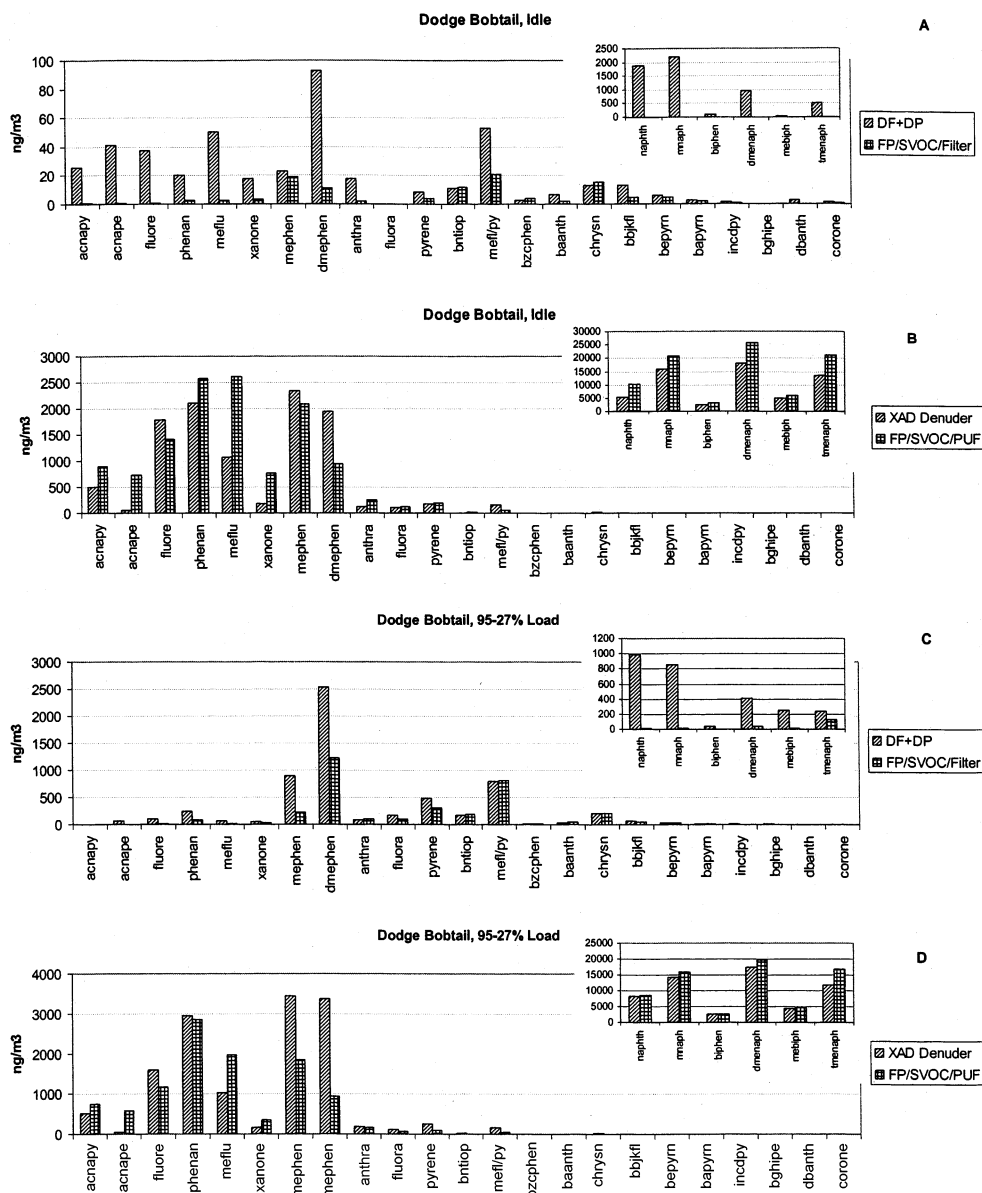


FIGURE 7. Comparison of samples collected with the denuder with samples collected in parallel with FP/SVOC sampler. (A) 1996 Dodge Bobtail, idle, denuder filter + denuder PUF/XAD/PUF vs FP/SVOC filter; (B) 1996 Dodge Bobtail, idle, denuder XAD portion vs. FP/SVOC PUF/XAD/PUF cartridge; (C) 1996 Dodge Bobtail, variable load, denuder filter + denuder PUF/XAD/PUF vs FP/SVOC filter; (D) 1996 Dodge Bobtail, high load, denuder XAD portion vs. FP/SVOC PUF/XAD/PUF cartridge.

Comparison of Denuder Sampler System and FP/SVOC Sampler. Figure 7A–D shows the comparison of samples collected with the denuder sampler and with the DRI FP/SVOC sampler for 1996 Dodge Bobtail idle and high load runs. The PUF/XAD/PUF extract from the FP/SVOC sampler is compared with the denuder extract (Figure 7B,D), and filter extract from FP/SVOC sampler is compared with denuder filter extract plus the extract from the PUF/XAD/PUF cartridge following the filter (Figure 7A,C). The most volatile two-ring PAHs are shown on the figure inserts. Their concentrations are approximately an order of magnitude higher than the concentrations of the most abundant three-ring PAH, and they show approximately 10–20% breakthrough the denuder. For semivolatile two- to four-ring PAHs, the sampling system consisting of a TIGF filter followed by a PUF/XAD/PUF cartridge (FP/SVOC sampler) showed lower concentrations on the filter and higher concentrations on the PUF/XAD/PUF cartridge in comparison with the denuder sampler, which indicates blow-off semivolatile PAH from the filter (negative sampling artifact) for the FP/SVOC system.

The exceptions are combined methyl- and dimethylphenanthrene isomers, for which the concentrations are generally higher for the denuder samples. The reason for this phenomenon is not clear—it may indicate breakthrough the PUF/XAD/PUF cartridge of FP/SVOC sampler or the presence of some interfering compounds on the XAD-coated denuder section of the annular denuder.

Figure 8 shows the same comparison for the gasoline-powered 1993 Ford F-350 run under high (53%) load (Figure 8A,B) and under variable (from 53% to 11%) load (Figure 8C,D). This vehicle shows generally low PM mass emission rates when compared with diesel vehicles tested (see Figure 1), and the total PM concentrations for high-load run was approximately 4 times lower than for variable low-load run. Figure 8 shows that the concentrations of the gas-phase 2-ring PAH for these two runs are comparable (or higher) than the diesel vehicle shown in Figure 7, but the concentrations of three-ring PAHs are lower. In addition, the concentration of five-ring PAHs and coronene are higher for this gasoline vehicle, especially for high load. This is consistent with a

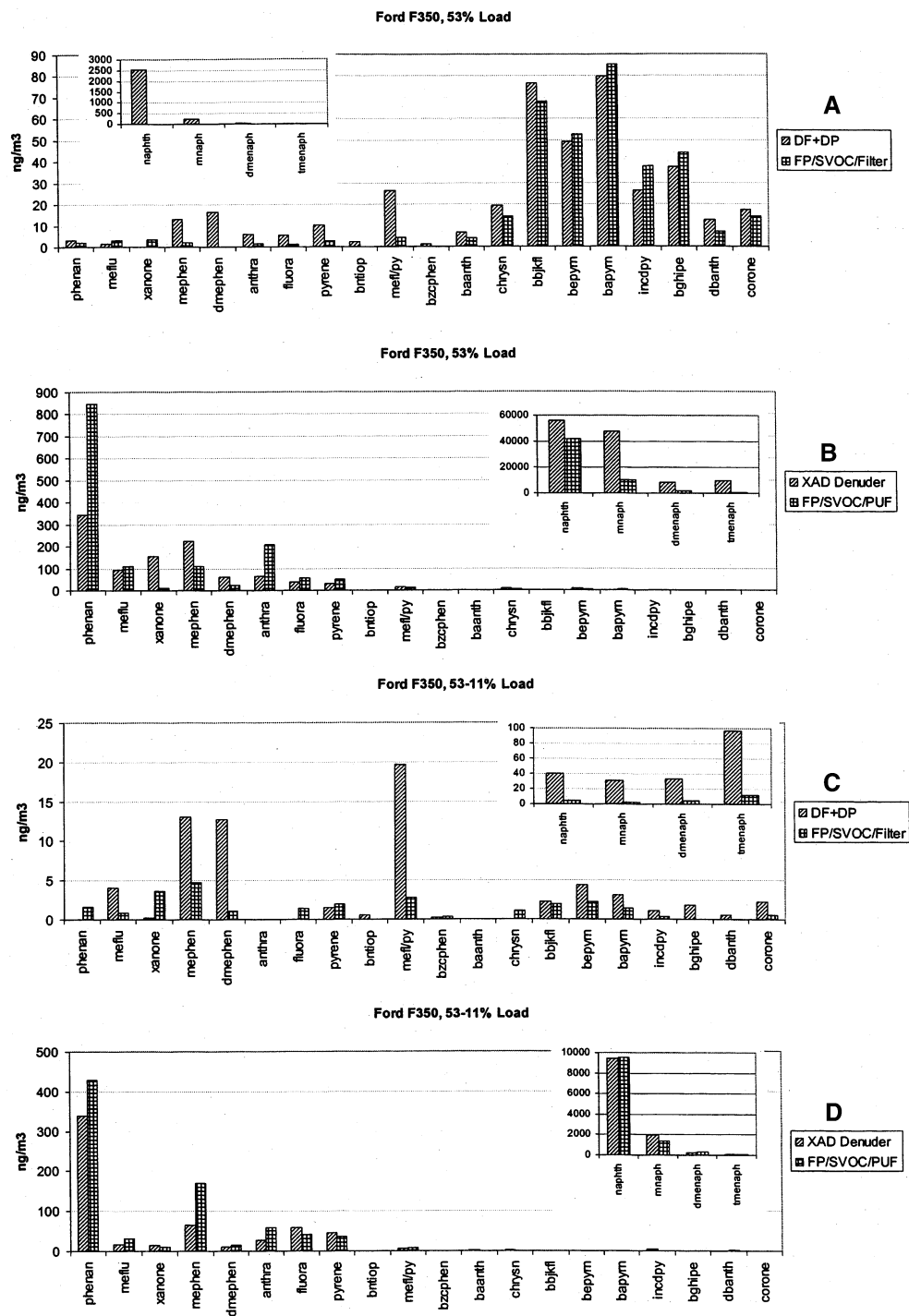


FIGURE 8. Comparison of samples collected with the denuder with samples collected in parallel with FP/SVOC sampler. (A) Ford F350, high load, denuder filter + denuder PUF/XAD/PUF vs FP/SVOC filter; (B) Ford F350, high load, denuder XAD portion vs. FP/SVOC PUF/XAD/PUF cartridge; (C) Ford F350, variable load, denuder filter + denuder PUF/XAD/PUF vs FP/SVOC filter; (D) Ford F350, variable load, denuder XAD portion FP/SVOC vs. PUF/XAD/PUF cartridge.

previous report (26). Again, for semivolatile two- to four-ring PAHs, the sampling system consisting of a TIGF filter followed by a PUF/XAD/PUF cartridge (FP/SVOC sampler) showed lower concentrations on the filter and higher concentrations on the PUF/XAD/PUF cartridge in comparison with the denuder sampler, which indicates blow-off semivolatile PAH from the filter (negative sampling artifact) for the FP/SVOC system. For diluted gasoline and diluted diesel exhaust, no evidence of positive filter artifact was observed. This indicates that the Teflon-coated glass fiber filters are less susceptible to gas-phase adsorption of volatile organic compounds than

glass fiber filters. Overall, the denuder sampling system provides a more accurate picture of the gas-particle phase distribution of semivolatile PAHs than a filter followed by a solid adsorbent.

Acknowledgments

This research was supported by Strategic Environmental Research and Development Program (SERDP) Project CP-1106, Characterization of Particulate Emission: Size Characterization and Chemical Speciation. We thank Mr. Bob Armstrong of Hill Air Force Base for his assistance and Dr.

Lara Gundel of Lawrence Berkeley National Laboratory (University of California, Berkeley) for denuder coating.

Literature Cited

- (1) Ligocki, M.; Pankow, J. F. *Environ. Sci. Technol.* **1989**, *23*, 75–83.
- (2) Pankow, J. F. *Atmos. Environ.* **1994**, *28* (2), 185–188.
- (3) Pankow, J. F. *Atmos. Environ.* **1994**, *28* (2), 189–194.
- (4) Odum, J. R.; Hoffman, T.; Bowman, F. A.; Collins, D.; Flagan, R. C.; Seinfeld, J. H. *Environ. Sci. Technol.* **1996**, *30* (8), 2580–2585.
- (5) Rogers, C. F.; Sagebiel, J. C.; Zielinska, B.; Arnott, W. P.; Fujita, E. M.; McDonald, J. D.; Griffin, J. B.; Kelly, K.; Overacker, D.; Wagner, D.; Lighty, J. S.; Sarofim, A.; Palmer, G. *Aerosol Sci. Technol.* **2003**, *37*, 355–368.
- (6) Kelly, K. E.; Wagner, D. A.; Lighty, J. S.; Sarofim, A. F.; Rogers, C. F.; Sagebiel, J.; Zielinska, B.; Arnott, W. P.; Palmer, G. *J. Air Waste Manage. Assoc.* **2003**, *53*, 273–282.
- (7) Hildemann, L. M.; Cass, G. R.; Markowski, G. R. *Aerosol Sci. Technol.* **1989**, *10*, 193–204.
- (8) Chan, T.; Lippmann, M. *Environ. Sci. Technol.* **1977**, *11* (4), 377–386.
- (9) Gundel, L. A.; Stevens, R. K.; Daisey, J. M.; Lee, V. C.; Mahanama, K. R. R.; Cancel-Velez, H. G. *Atmos. Environ.* **1995**, *29*(14), 1719–1733.
- (10) Arnott, W. P.; Moosmüller, H.; Rogers, C. F.; Jin, T.; Bruch, R. *Atmos. Environ.* **1999**, *33*, 2845–2852.
- (11) Moosmüller, H.; Arnott, W. P.; Rogers, C. F.; Bowen, J. L.; Gillies, J. A.; Pierson, W. R.; Collins, J. F.; Durbin, T. D.; Norbeck, J. M. *Environ. Sci. Technol.* **2001**, *35*, 1935–1942.
- (12) Arnott, W. P.; Zielinska, B.; Rogers, C. F.; Sagebiel, J.; Kelly, K. E.; Wagner, D. A.; Sarofim, A. F.; Lighty, J. S. *Aerosol Sci. Technol.* (submitted for publication).
- (13) U.S. EPA. Method TO-13, Revision 1.0, June 1988.
- (14) Chow, J. C.; Watson, J. G.; Pritchett, L. C.; Pierson, W. R.; Frazier, C. A.; Purcell, R. G. *Atmos. Environ.* **1993**, *27A*, 1185–1201.
- (15) Offenberg, J. H.; Baker, J. E. *Atmos. Environ.* **2002**, *36* (7), 1205–1220.
- (16) Possanzini, M.; Febo, A.; Liberti, A. *Atmos. Environ.* **1983**, *17* (12), 2605–2610.
- (17) Kamens, R. M.; Coe, D. L. *Environ. Sci. Technol.* **1997**, *31*, 1830–1833.
- (18) Yamanski, H.; Kuwata, K.; Miyamoto, H. *Environ. Sci. Technol.* **1982**, *16*, 189–194.
- (19) Pankow, J. F. *Atmos. Environ.* **1987**, *21* (11), 2275–2283.
- (20) Jang, M.; Kamens, R. M.; Leach, K. B.; Strommen, M. R. *Environ. Sci. Technol.* **1997**, *31* (10), 2805–2811.
- (21) McDow, S. R.; Sun, Q.; Vartiainen, M.; Hong, Y.; Yao, Y.; Fister, T.; Yao, R.; Kamens, R. M. *Environ. Sci. Technol.* **1994**, *28*, 2147–2153.
- (22) Kamens, R. M.; Odum, J. R.; Fan, Z. H. *Environ. Sci. Technol.* **1995**, *29* (1), 43–50.
- (23) Jang, M.; Kamens, R. M. *Environ. Sci. Technol.* **1998**, *32*, 2 (9), 1237–1243.
- (24) Dachs, J.; Eisenreich, S. J. *Environ. Sci. Technol.* **2000**, *34* (17), 3690–3697.
- (25) Kamens, R. M.; Jang, M.; Chien, C. J.; Leach, K. *Environ. Sci. Technol.* **1999**, *33* (9), 1430–1438.
- (26) Miguel, A. H.; Kirchstetter, T. W.; Harley, R. A.; Hering, S. V. *Environ. Sci. Technol.* **1998**, *32*, 450–455.

Received for review June 25, 2003. Revised manuscript received February 2, 2004. Accepted February 11, 2004.

ES030518D